

# Coded aperture correlation holography system with improved performance [Invited]

A. VIJAYAKUMAR, YUVAL KASHTER, ROY KELNER, AND JOSEPH ROSEN\*

Department of Electrical and Computer Engineering, Ben-Gurion University of the Negev, P.O. Box 653, Beer-Sheva 8410501, Israel

\*Corresponding author: rosenj@bgu.ac.il

Received 29 November 2016; revised 9 February 2017; accepted 9 February 2017; posted 9 February 2017 (Doc. ID 281764); published 8 March 2017

Coded aperture correlation holography (COACH) is a recently introduced technique for recording incoherent digital holograms of general three-dimensional scenes. In COACH, a random-like coded phase mask (CPM) is used as a coded aperture. Even though the CPM is optimized to reduce background noise, there is still a substantial amount of noise, mitigating the performance of COACH. In order to reduce the noise, we first modify the hologram reconstruction method. Instead of computing the correlation between a complex hologram of the entire object and a hologram of a source point, in this study the numerical correlation is performed with a phase-only filter. In other words, the phase function of the Fourier transform of the source point hologram is used as the spatial filter in the correlation process. Furthermore, we propose and demonstrate two additional methods for reducing the background noise in COACH. The first is based on the integration of a quadratic phase function, as used in Fresnel incoherent correlation holography (FINCH), with the CPM of COACH. This hybrid COACH-FINCH system enables a dynamic trade-off between the amount of background noise and the axial resolution of the system. The second method is employed by recording COACH holograms with multiple independent CPMs and averaging over the reconstructed images. The results of the above two techniques are compared with FINCH and with a regular imaging system. © 2017 Optical Society of America

**OCIS codes:** (090.1995) Digital holography; (110.0110) Imaging systems; (090.1760) Computer holography; (050.5080) Phase shift; (050.0050) Diffraction and gratings; (060.4785) Optical security and encryption.

<https://doi.org/10.1364/AO.56.000F67>

## 1. INTRODUCTION

Incoherent digital holography systems have various advantages as imaging systems: they can record and store a complete three-dimensional (3D) scene of objects radiating their own illumination [1,2], or objects illuminated by an incoherent natural light [3,4]. Furthermore, the recording process may be done with few camera exposures—at least three for in-line recorders [2–4], or even a single exposure for off-axis configurations [5,6]. Additionally, these imagers may be able to image targets through a scattering medium [7,8], or operate in a mode of synthetic aperture, such that object details can be resolved better than by equivalent imaging systems of similar physical aperture [9,10]. Unfortunately, according to several independent experiments [11,12] and a theoretical analysis [13], the axial resolution of these imagers is usually inferior to regular refractive-lenses-based imaging systems. While a low axial resolution, or, in other words, a large depth of focus [12], may be advantageous for certain applications, it can be a source of noise in other imaging applications. The practical implication of the low axial resolution in these imaging systems is that light from

out-of-focus object parts makes it difficult to observe, or to resolve, the desired in-focus parts. The axial resolution of incoherent digital holographic systems can be enhanced by an additional process of image sectioning [14–16] or by confocal holographic imaging [17,18], but the cost of these techniques is expressed by a loss in time resolution—a term that expresses, in the present context, the minimal time needed between two sequential acquired images, each of which is an image of a different state of the observed scene. In other words, all the sectioning techniques are implemented by slow scanning processes, which keep the systems from imaging dynamic scenes.

It is a challenge to develop an incoherent holographic system with an axial resolution similar to, or better than, that of a regular imaging system. Nevertheless, this desired system should keep, as much as possible, the abovementioned advantages of relatively fast operation and 3D imaging inherent to holographic imagers. Recently, an incoherent digital hologram recorder called a coded aperture correlation holography (COACH) was proposed [19]. COACH has the same axial resolution as a regular imager and the same time resolution as

holographic in-line recorder; i.e., at least three camera shots are required in order to properly recover the image from the hologram. COACH can be classified as an incoherent self-informative-reference holography system, in which the informative beam radiated from the object is split into two beams. One of these beams passes through a coded phase mask (CPM) displayed on a spatial light modulator (SLM). From the SLM, the beam propagates to the sensor plane, on which it interferes with the other beam that comes from the object without being modulated by the CPM. The intensity distribution of the two-beam interference is stored in the computer as a digital hologram of the object. Another hologram of a point object is recorded under the same conditions as before, and with the same CPM. This second hologram is used as the point spread function (PSF) in the digital reconstruction stage. Accordingly, the image is digitally reconstructed by correlating the object hologram with the PSF hologram.

The optical setup of COACH is similar to the setup of the Fresnel incoherent correlation holography (FINCH) system [2,3]. To a certain degree, FINCH can be considered as a special case of COACH, where the CPM is chosen as a quadratic phase function. In general, the CPM of COACH does not have this kind of limitation, and in principle, it can be any arbitrary phase function whose two-dimensional (2D) Fourier transform (i.e., its spatial spectrum) is also a phase function. The condition that both the CPM and its spatial spectrum are phase functions helps reduce the background noise level accompanying the reconstructed images [19], as is discussed more extensively in the following. Therefore, to fulfill this condition, the CPM of COACH is calculated using the iterative Gerchberg–Saxton algorithm (GSA) [20,21], such that it generates an approximately uniform intensity in the spatial spectrum. However, the background noise level, even with the iterative algorithm, is not tolerable, and other methods are needed to reduce the noise, as indeed are provided in the present study. It should be emphasized that the CPMs in our work are not limited to binary masks, as is the case with most of the traditional masks in coded aperture imaging systems [22,23]. The CPMs in the present study are multilevel pure-phase-valued masks similar to the masks proposed in [24]. As in [24], the phase values of the CPMs are computed by similar algorithms [20,21] and displayed directly on a pure-phase SLM without any further encoding process.

As mentioned above, the benefit of the improved axial resolution of COACH over FINCH does come at a cost. The hologram reconstruction of COACH may contain disturbing background random noise. To reduce the noise and to sharpen the reconstructed images, we first modify the method of reconstructing the image from the hologram. Inspired by the world of optical pattern recognition [25], the correlation between the object hologram and the PSF hologram is replaced with a numerical correlation, in which the type of spatial filter is a phase-only filter (POF) instead of the matched filter used in [19]. To further reduce the inherent noise of COACH, two different methods are proposed herein. The two proposed methods are different from each other in the type of penalty paid for improving the signal-to-noise ratio (SNR). In the first technique, a hybrid system is built by integrating COACH

with FINCH. According to this method, the SNR can be gradually increased at the cost of a corresponding reduction in the axial resolution, but the time resolution in this method is kept at the same high value as a common in-line holographic system. In the second approach, an averaging technique is employed to minimize the noise generated during the reconstruction. In this method, the SNR is enhanced on account of the time resolution, while keeping the axial resolution at the same high value as the original COACH.

In the next section, the methodology used for constructing the hybrid system and the averaging methods are discussed. The experimental analyses of all methods, and the comparison of their performance with FINCH and regular imaging systems, are presented in the Section 3. In the final section, the conclusion and summary of the research are presented.

## 2. METHODOLOGY

In this section, we describe two methods for reducing the reconstruction background noise associated with COACH, but first let's summarize the method of COACH, as introduced first in [19].

In COACH, two holograms are recorded under identical conditions, one for the observed object and another for a point object. The image of the object is reconstructed by correlating the above two holograms. For the reconstruction of thick objects from a COACH hologram, a prerecorded library of point object holograms for point objects located at different axial locations, corresponding to different axial planes of the objects, is required. We emphasize that this library need only be prepared once, offline, regardless of how many times objects are observed using the system. The process of in-line recording of holograms of general 3D objects is identical to the recording process of FINCH and many other self-reference on-axis digital hologram recorders, in the sense that at least three raw holograms of the scene are acquired. Since the reconstructed image is obtained as a result of a cross correlation between two random-like complex holograms, the image lateral and axial resolutions are dependent on the transverse and axial correlation lengths between the correlating functions [26,27], respectively.

The random-like nature of the CPM, besides providing a higher axial resolution for COACH, is also the cause for the background noise. To be precise, the main source of the background noise on the image plane is the algorithm of computing the CPM. As mentioned above, one of the GSA constraints is to have a uniform magnitude in the spatial spectrum domain. Recall that a reconstructed point is obtained as a result of autocorrelation of the complex hologram, and is based on the convolution theorem; this autocorrelation is equal to the Fourier transform of the squared magnitude of the spectral function. Therefore, as much as the magnitude of the spectral function is uniform, the point image is sharper with minimal sidelobes. However, it is well known that the GSA usually cannot satisfy both constraints simultaneously. Since the constraint in the CPM domain must be satisfied due to the use of a phase-only SLM, the other constraint in the spectral domain can only be approximated, but not completely satisfied. To the degree that the spectral magnitude is far from the constraint of being uniform, the sidelobes of the point image are higher and, as a

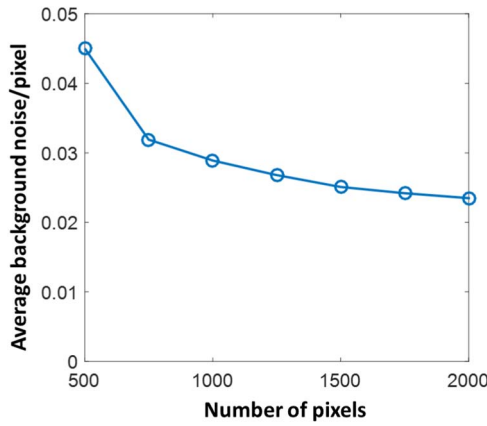


**Fig. 1.** Plot of the average background noise per pixel versus the size of the matrix.

result, the background noise is greater. To verify this assumption on the origin of the background noise, the following simulation was carried out. It is well known [20,21] that the constraints are better satisfied when the total number of matrix pixels in the GSA is higher. Therefore, if the noise is caused because the spectral constraint is not completely satisfied, then the noise is expected to be reduced by increasing the number of matrix pixels. The COACH holograms were simulated and reconstructed using CPMs with an increasing number of pixels. The plot of the average background noise per pixel for different values of the number of pixels is shown in Fig. 1. It can be noted that the average background noise indeed decreases with an increase in the number of pixels, indicating the origin of the background noise. The following subsections present two techniques to reduce this noise.

**A. Hybridization Method**

FINCH has been shown to have less background noise [19] than COACH. Hence, in order to reduce the background noise, we integrate the phase masks of COACH and FINCH into a single CPM, where a transition factor controls the level of hybridization between COACH and FINCH. By doing so, the noise can be reduced to any desired level between the noise levels of COACH and FINCH.

The optical configuration of the hybrid system for recording the object and pinhole holograms is shown in Fig. 2. The object is critically illuminated by an incoherent light source using the

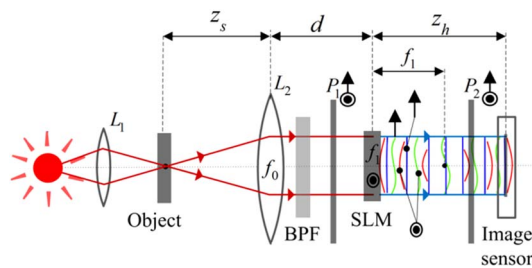


**Fig. 2.** Optical configuration of the system for recording hybrid COACH-FINCH holograms. The blue, red, and green wavefronts indicate plane, spherical, and quasi-random waves, respectively. BPF, bandpass filter;  $P_{1,2}$ , polarizers; SLM, spatial light modulator.

lens  $L_1$ . The light source is assumed to be spatially incoherent and quasi-monochromatic, so that the light emitted from each point on the object is only coherent with itself. A second lens  $L_2$  is placed at a distance of  $z_s$  from the object, to collimate the light diffracted by the object. A polarizer  $P_1$  is used to orient the light field to an angle of  $45^\circ$  with respect to the active axis of the SLM. A hybrid phase mask, consisting of a combination of the quadratic phase function of FINCH and the CPM of COACH, is displayed on the SLM [see Eq. (1) below]. Since the light incident on the SLM is polarized at  $45^\circ$  with respect to the active axis of the SLM, only about half of the intensity of the incident light is modulated by the hybrid CPM displayed on the SLM, while the remaining intensity propagates unmodulated. To create interference between the above two orthogonal polarizations, a second polarizer  $P_2$ , with an orientation of  $45^\circ$  with respect to the active axis of the SLM, is mounted after the SLM. The interference pattern is recorded by a digital camera for further digital processing. Only the beams originating from the same point on the object are coherently interfered. This optical configuration is both compact and robust [28]. A phase-shifting technique, which involves the recording of three holograms with different phase values  $\theta = 0^\circ, 120^\circ,$  and  $240^\circ$ , is used to cancel the zeroth-order term and the twin image. These three holograms are superposed to yield the complex hologram  $H_{OBJ}$  [19]. The reconstruction method of the object hologram is similar to the methods proposed in optical scanning holography [29] and self-interference incoherent digital holography [30], in order to minimize the error between the reconstructed and original images in both cases. Instead of reconstructing the hologram via by standard Fresnel backpropagation integral, it is digitally correlated with a version of the complex hologram of a point object. In our case, the same recording process is performed for a point object implemented by a pinhole and located at the exact same axial location as the 2D object, or a single section of the 3D object, to be stored in the hologram. The obtained complex hologram of the pinhole, after completing the hereafter described numerical procedure, is designated as  $\tilde{H}_{PSF}$ . The image is digitally reconstructed by a correlation between the above two complex-valued holograms  $H_{OBJ}$  and  $\tilde{H}_{PSF}$ . The hologram  $H_{OBJ}$  recorded by this hybrid system is a superposition of shifted and scaled functions, which are a mix of quadratic and random-like functions; hence,  $H_{OBJ}$  has the properties of both FINCH and COACH. The hybrid CPM, realized directly and without any encoding, using a phase-only SLM, is

$$t_k(\vec{r}) = Q\left(\frac{-1}{f_1}\right) \exp[i\alpha\Phi(\vec{r})] \exp(i\theta_k), \quad k = 1, 2, 3, \quad (1)$$

where  $Q$  designates the quadratic phase function  $Q(b) = \exp[i\pi b\lambda^{-1}(x^2 + y^2)]$  and  $\lambda$  is the central wavelength of the light source. The angle  $\theta_k$  is one of the three phase shifts used for the elimination of the twin image and the bias terms from the final hologram [2,3]. The function  $\Phi(\vec{r})$  represents the quasi-random phase calculated using the GSA [19–21], to generate a uniform magnitude in the spectrum domain of the CPM. The part of FINCH in the CPM is similar to FINCH of Ref. [31], in which the focal length  $f_1$  of the quadratic phase function is selected to be half of the distance  $z_b$  between the SLM and the image sensor. This selection is made to

obtain a complete overlap between the two interfering waves originating from the same object point, and consequently to achieve the highest lateral image resolution [31]. By tuning the transition factor  $\alpha$ , the hybrid CPM can be set to different hybridization levels, from the quadratic phase function of FINCH ( $\alpha = 0$ ) to the pseudorandom CPM ( $\alpha = 1$ ) of COACH. By giving  $\alpha$  intermediate values between 0 and 1, the hybrid system possesses mixed properties of both FINCH and COACH. In order to enable high visibility of the interference between two waves propagating through the system along two different paths, the maximal optical path difference should be smaller than the temporal coherence length [32]. To guarantee this condition, a bandpass filter is introduced after lens  $L_2$ . Based on Fig. 2, if the complex amplitude before lens  $L_2$  is given by a quadratic phase function  $Q(1/z_s)$ , the complex amplitude after lens  $L_2$  is given by  $Q(1/z_s) \cdot Q(-1/f_0)$ . The complex amplitude just before the SLM, a distance  $d$  from lens  $L_2$ , is calculated by a convolution of  $Q(1/z_s) \cdot Q(-1/f_0)$  with the quadratic phase function  $Q(1/d)$ . The complex amplitude just after the SLM is the product of the complex amplitude before the SLM and the hybrid phase mask  $t_k$ , given by Eq. (1), plus a constant  $C_2$  representing the second beam, which is not modulated by the SLM. The resulting complex amplitude from the SLM is convolved with  $Q(1/z_b)$  to calculate the complex amplitude on the image sensor, at a distance  $z_b$  from the SLM. As a result, taking into consideration the well-known Fresnel approximation, the hologram of an object point (i.e., a pinhole) located at  $(0, 0, -z_s)$  with an amplitude of  $\sqrt{I_s}$  can be formulated as follows:

$$I_k(\vec{r}_0) = \left| \sqrt{I_s} C_1 Q\left(\frac{1}{z_s}\right) Q\left(-\frac{1}{f_0}\right) * Q\left(\frac{1}{d}\right) [t_k(\vec{r}) + C_2] * Q\left(\frac{1}{z_b}\right) \right|^2 \quad k = 1, 2, 3, \quad (2)$$

where the asterisk sign denotes a 2D convolution,  $C_1$  is a complex constant, and  $\vec{r}_0 = (u, v)$  is the transverse location vector in the sensor plane. For simplicity, and without loss of generality, the analysis is given for the special case in which the distance  $d$  between the lens  $L_2$  and the SLM is zero. This can be achieved approximately by attaching  $L_2$  to the SLM or precisely, and more practically, by use of an optical relay system that projects the plane of  $L_2$  onto the SLM plane [33]. In either case, Eq. (2) can be simplified as follows:

$$I_k(\vec{r}_0) = \left| \sqrt{I_s} C_1 Q\left(\frac{1}{z_1}\right) [t_k(\vec{r}) + C_2] * Q\left(\frac{1}{z_b}\right) \right|^2, \quad (3)$$

where  $z_1 = z_s f_0 / (f_0 - z_s)$ . Substituting Eq. (1) into Eq. (3), the intensity distribution is

$$I_k(\vec{r}_0) = \left| \sqrt{I_s} \left[ C_1 Q\left(\frac{1}{z_2}\right) \exp[i\alpha\Phi(\vec{r})] \exp(i\theta_k) * Q\left(\frac{1}{z_b}\right) + C_2 Q\left(\frac{1}{z_3}\right) \right] \right|^2, \quad (4)$$

where  $z_2 = z_1 f_1 / (f_1 - z_1)$  and  $z_3 = z_1 + z_b$ . It is assumed that the combination of two types of phase functions displayed on the SLM induces two different waves on the sensor plane. This assumption is understood if the term of the

COACH-CPM is written as a power series as follows:  $\exp[i\alpha\Phi(\vec{r})] = 1 + i\alpha\Phi(\vec{r}) - \alpha^2[\Phi(\vec{r})]^2/2 \dots$ . Thus, on the sensor plane the complex amplitude is approximately a superposition of three components as follows:

$$I_k(\vec{r}_0) = \left| \sqrt{I_s} \left[ C_0 \exp(i\theta_k) \left\{ \sqrt{1 - \alpha^2} Q\left(\frac{1}{z_4}\right) + \alpha G'(\vec{r}_0) \right\} + C_2 Q\left(\frac{1}{z_3}\right) \right] \right|^2, \quad (5)$$

where  $z_4 = z_b + z_2$  and  $C_0$  is a constant. The function  $G'$  is the complex amplitude obtained after free-space propagation from the part of the COACH-CPM along a distance  $z_b$  to the sensor plane. Following the phase-shifting procedure, the distribution of the complex PSF hologram is

$$H_{\text{PSF}}(\vec{r}_0) = C \left\{ \sqrt{1 - \alpha^2} Q\left(\frac{1}{z_r}\right) + \alpha G(\vec{r}_0) \right\}, \quad (6)$$

where  $z_r = z_4 z_3 / (z_3 - z_4)$ ,  $G(\vec{r}_0) = G'(\vec{r}_0) Q(-1/z_3)$ , and  $C$  is a complex constant.

In general, there is a strong analogy between the process of reconstructing an image from the COACH hologram and pattern recognition by optical correlators [25]. In both cases, the goal is to get as sharp as possible a correlation peak at the output of the system whenever there is a true object somewhere on the input plane of the pattern recognizer [25], or whenever there is a complex PSF hologram somewhere on the hologram plane in the case of COACH. Based on this analogy, we modified the reconstruction process in COACH by filtering the spatial spectrum of the hologram with a POF. Since a POF does not amplify or attenuate any part of the hologram spectrum, the correlation peaks are more intense, and the ratio of peak-to-sidelobes is higher, than in the case of correlation with a matched filter [25]. However, it is not argued in this study that the POF is the optimal filter for reconstructing holograms, and further research for optimizing the sharpness of the correlation peaks should be done in the future.

The reconstructed image of the object point is obtained as a correlation of  $H_{\text{PSF}}$  with the inverse Fourier transform of the POF as follows:

$$\begin{aligned} T(\vec{\rho}) &= \iint H_{\text{PSF}}(\vec{r}_0) \tilde{H}_{\text{PSF}}^*(\vec{r}_0 - \vec{\rho}) du' dv' \\ &\approx \sqrt{1 - \alpha^2} Q\left(\frac{1}{z_r}\right) \otimes Q\left(\frac{1}{z_r}\right) + \alpha G(\vec{\rho}) \otimes \tilde{G}(\vec{\rho}) \\ &= \sqrt{1 - \alpha^2} h_F(\vec{\rho}) + \alpha h_C(\vec{\rho}), \end{aligned} \quad (7)$$

where

$$\tilde{H}_{\text{PSF}}(\vec{\rho}) = \mathfrak{F}^{-1}\{\exp[i \cdot \arg\{H_{\text{PSF}}(\vec{\rho})\}]\}$$

and

$$\tilde{G}(\vec{\rho}) = \mathfrak{F}^{-1}\{\exp[i \cdot \arg\{\mathfrak{F}\{G(\vec{\rho})\}\}]\}.$$

The sign  $\otimes$  indicates 2D correlation,  $\mathfrak{F}$  and  $\mathfrak{F}^{-1}$  stand for 2D Fourier and inverse Fourier transforms, respectively, and  $\vec{\rho}$  is the location vector in the reconstruction plane. Note that the cross correlation terms between  $G$  and  $Q$  have been neglected in Eq. (7), which is allowed under the assumption that  $G$  has the nature of a random zero-mean function [19]. The

term  $h_F$  in Eq. (7) is well known from previous studies [2,3,31] as the focal spot of a lens with a focal length of  $z_r$ . Assuming the aperture of the system at the SLM plane is a disk of diameter  $D$ , then  $h_F(\tilde{\rho}) = 2J_1(\pi D\rho/\lambda z_r)/(\pi D\rho/\lambda z_r)$ . The width of  $h_F$  is  $1.22\lambda z_r/D$ .  $h_C$  is the cross correlation function of  $G$  with  $\tilde{G}$ . Since it is assumed that  $G$  and  $\tilde{G}$  have the nature of a random zero-mean function,  $h_C$  is a narrow delta-like function with a width of the correlation length and random, relatively low side-lobes. The lateral correlation length is determined by the smallest spot that can be obtained on the sensor plane by the SLM, which is about  $1.22\lambda z_b/D$ . It should be noted that the values of  $h_F$  and  $h_C$  are generally not the same. In the special case where  $z_s = f_o$ , it is easy to see that  $z_r = z_b/2$ , and hence the size of  $h_F$  can be half the size of  $h_C$ .

An arbitrary incoherently illuminated 2D object  $o(x, y)$  can be represented as a collection of  $N$  uncorrelated radiating points as follows:

$$o(x, y) = \sum_j^N a_j \delta(x - x_j, y - y_j). \quad (8)$$

Assume that the object replacing the pinhole is located at the same distance  $z_s$  mentioned above. Each incoherent object point  $j$  induces three mutually coherent beams on the sensor plane (Fig. 2). One beam is not modulated by the SLM and arrives at the sensor as an inclined spherical wave of the form  $A_j \exp[i2\pi(ux_j + vy_j)/\lambda z_s]Q(1/z_3)$ . The beam modulated by the quadratic phase part on the SLM arrives on the sensor as a different inclined spherical wave of the form  $A_j \exp[i2\pi(ux_j + vy_j)z_5/\lambda z_4 z_s]Q(1/z_4)$ , where  $z_5 = z_b - z_4$ . The other modulated beam is a shifted version of  $G(u, v)$  multiplied by a plane wave. Formally, this last beam is represented as  $\exp[i2\pi(ux_j + vy_j)/\lambda z_s]G(u - u_j, v - v_j)$ , where  $\tilde{r}_j = (u_j, v_j) = (x_j, y_j)z_b/z_s$ . Consequently, the overall intensity distribution on the sensor plane, due to the entire object, is

$$I_k(u, v) = \sum_j \left| A_j \exp\left[\frac{i2\pi(x_j u + y_j v)}{\lambda z_s}\right] Q\left(\frac{1}{z_3}\right) + B_j \exp(i\theta_k) \times \left\{ \sqrt{1 - \alpha^2} \exp\left[\frac{i2\pi z_5(x_j u + y_j v)}{\lambda z_4 z_s}\right] Q\left(\frac{1}{z_4}\right) + \alpha \exp\left[\frac{i2\pi(x_j u + y_j v)}{\lambda z_s}\right] G'(\tilde{r}_o - \tilde{r}_j) \right\} \right|^2, \quad (9)$$

where  $A_j$  and  $B_j$  are complex constants. The complex hologram obtained from the phase-shifting procedure is

$$H_{\text{OBJ}}(u, v) = \sqrt{1 - \alpha^2} \sum_j A_j^* B_j \exp\left[\frac{i2\pi z_b(x_j u + y_j v)}{\lambda z_4 z_s}\right] Q\left(\frac{1}{z_r}\right) + \alpha \sum_j A_j^* B_j G(\tilde{r}_o - \tilde{r}_j). \quad (10)$$

The image reconstruction is carried out by correlating the complex PSF hologram  $\tilde{H}_{\text{PSF}}$  and the complex object hologram  $H_{\text{OBJ}}$  as follows:

$$P(u', v') = \iint H_{\text{OBJ}}(u, v) \tilde{H}_{\text{PSF}}^*(u - u', v - v') du dv \approx \sqrt{1 - \alpha^2} \sum_j A_j^* B_j h_F(u' - u_j, v' - v_j) + \alpha \sum_j A_j^* B_j h_C(u' - u_j, v' - v_j) \propto o(u'/M_T, v'/M_T). \quad (11)$$

The resulting image is a magnified image of the object, with a transverse magnification of  $M_T = z_r z_b/(z_4 z_s)$ , which can be  $M_T = z_b/f_o$  in the case where  $z_s = f_o$ . Note that for any point  $j$ , both  $h_F$  and  $h_C$  are imaged into  $\tilde{r}_j = (u_j, v_j)$  with the same lateral magnification  $M_T$ , although the values of  $h_F$  and  $h_C$  are not necessarily the same. In other words, the spot magnifications  $M_W$  of FINCH and COACH are not necessarily equal, although their lateral magnifications  $M_T$  are always equal. The spot magnification  $M_W$  is the ratio between the widths of the minimal resolved spots at the image and object planes.  $M_W$  can be easily calculated as the ratio between the numerical apertures at the object and image planes. In the case of COACH, both magnifications are equal, i.e.,  $M_T = M_W$ , similar to classical imagers. However, with FINCH the case is different; in the case of maximum resolution, in which  $z_s = f_o$  and  $z_b = 2f_1$ , the lateral magnification is  $M_T = z_b/f_o = 2f_1/f_o$ , whereas the spot magnification is  $M_W = f_1/f_o$ . Therefore, the magnification equation becomes  $M_T = 2M_W$ . Recalling that a possible formal manifestation of the Lagrange invariant is the equality  $M_T = M_W$  [13], one realizes that the Lagrange invariant can be violated in a FINCH system. On the same optical configuration shown in Fig. 2, one part of the system, the part related to COACH, always obeys the Lagrange invariant, whereas the other part, related to FINCH, may violate the Lagrange invariant. Hence, the hybrid system may also violate the Lagrange invariant, except for the case when  $\alpha = 1$ , i.e., when the system is purely COACH.

The similarity between COACH and classical imaging systems in the lateral resolution is valid also for the axial resolution. For COACH, the axial resolution is determined by the axial width of the pinhole image, which is dictated by the axial correlation length. Since the axial length of the smallest spot on the sensor is  $\sim 16\lambda(z_b/D)^2$ , the minimum resolved axial size in the object is  $\sim 8\lambda(f_o/D)^2 = 2\lambda/(\text{NA})^2$ , which is about the same resolution limit as for a conventional imager [34]. On the other hand, as discussed in [13], FINCH has a poorer axial resolution than both the classical imaging system and COACH. This trade-off between noise level and axial resolution is exploited by the proposed hybrid system. Explicitly, higher values of  $\alpha$  toward 1 mean that the system is closer to COACH, in the sense that the axial resolution and the noise level are both higher, whereas lower values of  $\alpha$  toward 0 mean that the system is closer to FINCH, in the sense that the axial resolution and the noise level are both lower.

### B. Averaging Method

The theoretical description of the second technique, known as the averaging COACH, is presented in this section. The

background noise in the reconstructed images of COACH is reduced at the expense of the time resolution of the system.

The method of averaging COACH is based on the assumption that every two CPMs of COACH, each synthesized from a different independent random matrix, are not correlated to each other. In other words, the value of their cross correlation is negligible in comparison to the peak values of their autocorrelations. Under this assumption, one can deduce that the random-like nature of the CPMs is transferred to the functions  $G_s$ , which are diffracted from the CPMs and measured on the sensor plane. Hence, for an infinite number of  $S$  independent CPMs, the series of background noise values  $U_j(s) = \int G_s(\bar{r}_o) G_s^*(\bar{r}_o - \bar{r}_j) d\bar{r}_o$  at some point  $j$ , far more than the correlation length from the autocorrelation peak on the sensor plane, is a random zero-mean, complex-valued series. Therefore, recording  $S$  independent COACH complex holograms, each of which is related to a different independent CPM, and averaging over all  $S$  reconstruction planes in their complex state (before taking the absolute value of the plane distribution) reduces the background noise toward zero as  $S$  goes toward an infinite number of holograms. This noise reduction can be achieved while preserving the intrinsic axial resolution of COACH. However, the penalty of this method is expressed by a low time resolution; instead of recording three raw holograms, one needs to record  $3S$  holograms. It should be emphasized that each reconstruction is realized using a POF in the  $s$  digital correlator, as described in Section 2.A.

The SNR on the reconstruction plane is defined as the ratio between the mean value and the standard deviation [35] of the reconstructed image. To analyze the improvement in the SNR from increasing the  $S$  independent COACH holograms, the noise ratio between the SNR for some  $S$  and the SNR for  $S = 1$  is defined as follows:

$$\frac{\text{SNR}_S}{\text{SNR}_1} = \frac{\sigma_1}{\sigma_S} = \frac{\sqrt{\frac{1}{MN} \sum_{m=1}^M \sum_{n=1}^N |P_1(m, n) - \bar{P}(m, n)|^2}}{\sqrt{\frac{1}{MN} \sum_{m=1}^M \sum_{n=1}^N |P_S(m, n) - \bar{P}(m, n)|^2}}, \quad (12)$$

where  $\bar{P}(m, n)$  is the ideal image without noise,  $\sigma_s$  is the standard deviation of the averaged reconstructed images over  $S$  images, and  $P_S(m, n)$  is the average over  $S$  reconstructed images, given by  $P_S(m, n) = \sum_{s=1}^S P_s(m, n)/S$ . The value of the mean is the same for any  $S$  and therefore is canceled in Eq. (12). Reference [35] indicates that for independent  $S$  images, the SNR should be improved by the factor  $\sqrt{S}$  in comparison to  $\text{SNR}_1$ . This signal-to-noise improvement of the averaging COACH can be achieved without giving away the axial resolution of COACH, but at the expense of an increased number of camera shots and therefore a longer recording and processing time.

### 3. EXPERIMENTS

The two noise reduction techniques are experimentally demonstrated using the setup shown in Fig. 3, which is similar to the experimental setup of [19]. Two illumination channels were used, each with a light-emitting diode (LED) (Thorlabs LED631E, 4 mW,  $\lambda = 635$  nm,  $\Delta\lambda = 10$  nm). Two identical lenses  $L_{1A}$  and  $L_{1B}$  were mounted in channels 1 and 2,

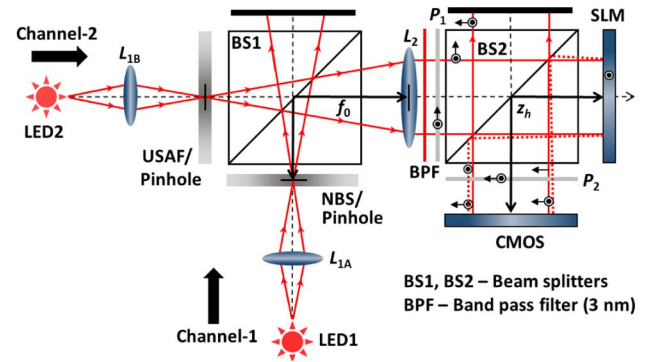


**Fig. 3.** Experimental setup of COACH with two illumination channels.

respectively, to critically illuminate the objects [36]. The distance between the lenses  $L_{1A}$  and  $L_{1B}$  and the respective objects is 3 cm, and the diameter of the beam at the output of the lens is  $\sim 0.4$  cm, imposing an NA of  $\sim 0.067$ . Hence, the lateral resolution is roughly  $6 \mu\text{m}$  ( $0.61\lambda/\text{NA}$ ) and the axial resolution is about  $0.28$  mm [ $2\lambda/(\text{NA})^2$ ]. A beam splitter (BS1) was used to combine the light from the two channels. The light diffracted by the objects in the two channels is incident on lens  $L_2$  with a focal length of  $f_0 = 20$  cm, mounted at a distance of about 20 cm from the two objects. The light diffracted from the two objects is collimated by the lens  $L_2$ , and is polarized by the polarizer  $P_1$  oriented at an angle of  $45^\circ$  with respect to the active axis of the SLM (Holoeye PLUTO,  $1920 \times 1080$  pixels,  $8 \mu\text{m}$  pixel pitch, phase-only modulation). About half of the light intensity oriented along the direction of the active axis of the SLM is modulated, while the remaining intensity propagates without being modulated. The SLM is placed at a distance of 11 cm from the lens  $L_2$ . The distance between the second beam splitter (BS2) and the SLM is 5 cm. A second polarizer  $P_2$ , oriented also at  $45^\circ$  with respect to the orientation of the SLM, was used to enable the pass and interference only between components with the same orientation. The interference is recorded by a digital camera (Hamamatsu ORCA-Flash4.0 V2 Digital CMOS,  $2048 \times 2048$  pixels,  $6.5 \mu\text{m}$  pixel pitch, monochrome). The distance between the SLM and the camera is  $z_h = 40$  cm. The distance values were selected to implement FINCH in an optimal configuration in the sense of maximum lateral resolution, similar to Ref. [31]. As per the phase-shifting method, CPMs corresponding to  $\theta = 0^\circ$ ,  $120^\circ$ , and  $240^\circ$  were displayed in the SLM to eliminate the twin image and the zeroth-order terms [2,3].

#### A. Experimental Results of Hologram Reconstruction with a POF

In the first experiment, we investigate the differences between the previous reconstruction method [19] and the proposed one, based on a POF. A complex hologram was recorded with the 10 line pairs per mm (lp/mm) element of a negative National Bureau of Standards (NBS) chart. Its reconstructions using a POF and a matched filter are compared in Fig. 4. It is clearly observed that the POF-based reconstruction is sharper and has much less background noise when compared to the matched-filter-based reconstruction.

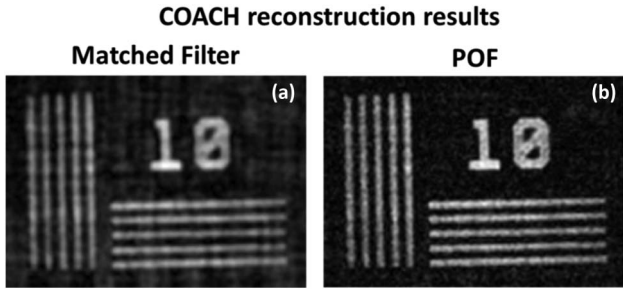


**Fig. 4.** Reconstruction results for a COACH hologram of an object (Element 10 lp/mm of the NBS chart) with (a) a matched filter and (b) a POF.

**B. Experimental Results of the Hybridization Technique**

In the hybridization technique, the quadratic phase function of FINCH is integrated with the CPM of COACH as described in Section 2.A. By gradually varying the value of  $\alpha$  from 0 to 1, the degree of hybridization is varied from pure FINCH ( $\alpha = 0$ ) to pure COACH ( $\alpha = 1$ ). For this study, hybrid systems with  $\alpha = 0, 0.2, 0.4, 0.6, 0.8,$  and  $1$  were tested. The CPM of COACH was calculated using the GSA, while the focal distance of the FINCH diffractive lens was  $f_1 = z_b/2 = 20$  cm. In the first experiment, a pinhole ( $25 \mu\text{m}$ ) was mounted on one of the channels at the front focal plane of lens  $L_2$ , while the other channel was blocked, and a hologram  $H_{\text{PSF}}$  of the pinhole was recorded for the above values of  $\alpha$ . The location of the pinhole varied from an axial distance of  $-8$  cm to  $+8$  cm with respect to the front focal plane of lens  $L_2$ . The holograms  $H_{\text{PSF}}$  (for  $\theta = 0^\circ, 120^\circ$  and  $240^\circ$ ) were recorded for the different values of  $\alpha$  and different axial locations, but with the same components ( $\Phi(\vec{r})$  and  $Q(-1/f_1)$ ) of the hybrid CPM. The phase images of the phase masks displayed on the SLM for  $\alpha = 0, 0.2, 0.4, 0.6, 0.8$  and  $1$  are shown in Figs. 5(a)–5(f), respectively. The holograms of the pinhole, for  $\theta = 0^\circ, z_s = f_o$ , and for the above values of  $\alpha$  are shown in Figs. 6(a)–6(f), respectively.

The holograms  $H_{\text{PSF}}$  recorded at different axial locations were correlated with the  $\tilde{H}_{\text{PSF}}$  recorded at the front focal plane of lens  $L_2$  ( $z_s = f_o$ ) and the intensity of the reconstructed image at  $(x, y) = (0, 0)$  was measured. The axial resolution of the hybrid systems for different values of  $\alpha$  was analyzed by plotting the intensity of the reconstructed image at  $(x, y) = (0, 0)$  with respect to the axial position of the pinhole object. The experiment was carried out for a regular imager by measuring the intensity of the image at  $(x, y) = (0, 0)$ , whereas the pinhole at the locations of  $z_s - f_o = \pm 8$  cm was imaged with a diffractive lens displayed on the SLM with a focal length of  $f_1 = z_b = 40$  cm. The plots of the point image at  $(x, y) = (0, 0)$  versus the axial location of the pinhole for regular imaging, for FINCH, and for the hybrid system with different values of  $\alpha$  are shown in Fig. 7.

In Fig. 7, it can be seen that the curve of COACH matches well with that of regular imaging, as was also demonstrated earlier [19]. In the hybrid systems for  $\alpha = 0$  to  $1$ , the profile of the normalized intensity at  $(x, y) = (0, 0)$  reveals the gradual increase in the axial resolution of the system, from the lowest axial

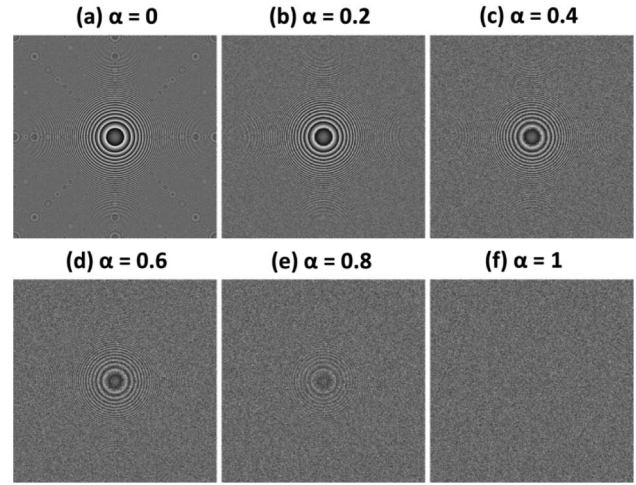


**Fig. 5.** Images of the SLM-displayed phase masks for (a)  $\alpha = 0$ , (b)  $\alpha = 0.2$ , (c)  $\alpha = 0.4$ , (d)  $\alpha = 0.6$ , (e)  $\alpha = 0.8$ , and (f)  $\alpha = 1$ .

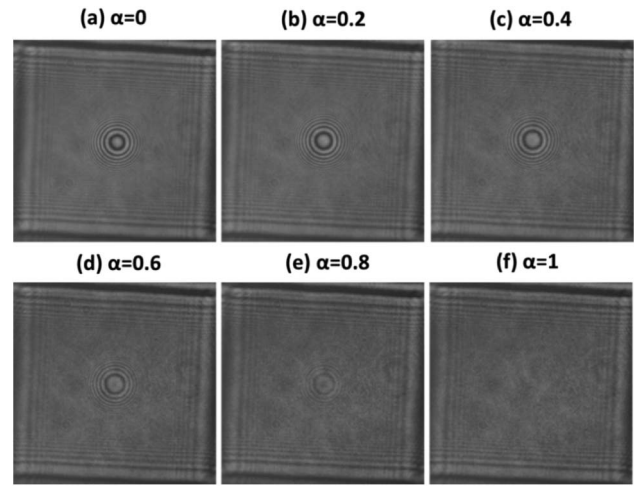


**Fig. 6.** Images of the raw holograms of the pinhole for a phase-shift value of  $\theta = 0^\circ$  for (a)  $\alpha = 0$ , (b)  $\alpha = 0.2$ , (c)  $\alpha = 0.4$ , (d)  $\alpha = 0.6$ , (e)  $\alpha = 0.8$ , and (f)  $\alpha = 1$ .

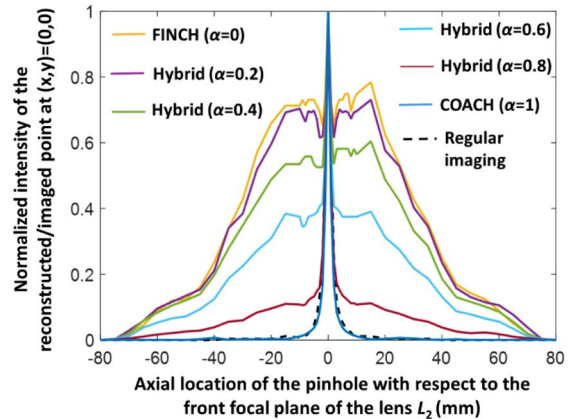


**Fig. 7.** Normalized intensity of the reconstructed/imaged point at  $(x, y) = (0, 0)$  for different axial distances of the pinhole for regular imaging, FINCH, and the hybrid system with different  $\alpha$  values.

resolution for  $\alpha = 0$  up to the maximum axial resolution for  $\alpha = 1$ .

To understand the behavior of the hybrid systems in a more practical case, two targets, namely the NBS (NBS 1963A Thorlabs) and United States Air Force (USAF) charts (USAF 1951 1X Edmund Optics) were mounted in channel 1 and channel 2, respectively. Element 10 lp/mm of the NBS chart and elements 4 (11.31 lp/mm), 5 (12.70 lp/mm), and 6 (14.25 lp/mm) of group 3 in the USAF chart were illuminated in a similar way. In these two resolution charts, the other group elements were masked out. In the experiment, the axial location of the NBS resolution chart in channel 1 was fixed, while the axial location of the USAF resolution chart in channel 2 was varied from  $\Delta = -3$  cm to  $+3$  cm with respect to the front focal plane of lens  $L_2$ . The holograms of the two objects,  $H_{\text{OBJ}}$ , were recorded at every new axial location of the USAF resolution chart for different values of  $\alpha$ . At each axial location, and for each value of  $\alpha$ , three holograms  $H_{\text{OBJ}}$ , with the abovementioned three phase-shift values, were recorded and superposed as explained above. The images of the two objects at the above different axial locations of the USAF resolution chart were also imaged directly by the regular imaging system. The experiment was repeated by blocking channel 1 and replacing the USAF resolution chart in channel 2 with a pinhole such that the holograms  $H_{\text{PSF}}$  for different values of  $\alpha$ , but with the same hybrid CPM, were recorded at the corresponding locations to the USAF holograms  $H_{\text{OBJ}}$ . The images of the objects at different axial locations were reconstructed by correlating the holograms  $H_{\text{OBJ}}$  with the  $\tilde{H}_{\text{PSFS}}$  recorded at the corresponding axial positions. Hence, the hologram  $H_{\text{OBJ}}$  of the two objects was reconstructed using two  $\tilde{H}_{\text{PSFS}}$  corresponding to the axial locations of the two planes of the objects. In the case of regular imaging, the imaging at different planes was carried out by varying the focal distance of the diffractive lens displayed on the SLM such that the respective planes were in focus, while the other planes were out of focus. The overall results of imaging/reconstruction are shown in Fig. 8. It can be noted that the axial resolution of the system and the background noise level increased with the increase in the value of  $\alpha$  from 0 to 1. Therefore, with a suitable choice of the value of  $\alpha$ , it is possible to transit the system from an almost noiseless low-axial-resolution FINCH to a noisy high-axial-resolution COACH.

As a result of the Lagrange invariant violation by FINCH mentioned in Section 2.A, the lateral resolution of FINCH is about 1.5 times better than that of an equivalent incoherent imaging system [31]. In the case of COACH, the lateral resolution is theoretically the same as that of a regular imaging system [19]. However, in our present experimental setup, the theoretical resolution (6  $\mu\text{m}$  in the present setup) has not been achieved due to the use of a pinhole wider than the smallest size the system can resolve. The reconstruction resolution of the object can be improved when the diameter of the pinhole is decreased. Resolution enhancement was noted when the pinhole size was decreased from 100 to 25  $\mu\text{m}$ . When the reconstruction of the hybrid holograms was carried out using Fresnel backpropagation for smaller values of  $\alpha$  (0–0.6), the lateral resolution matched that of FINCH reconstruction,

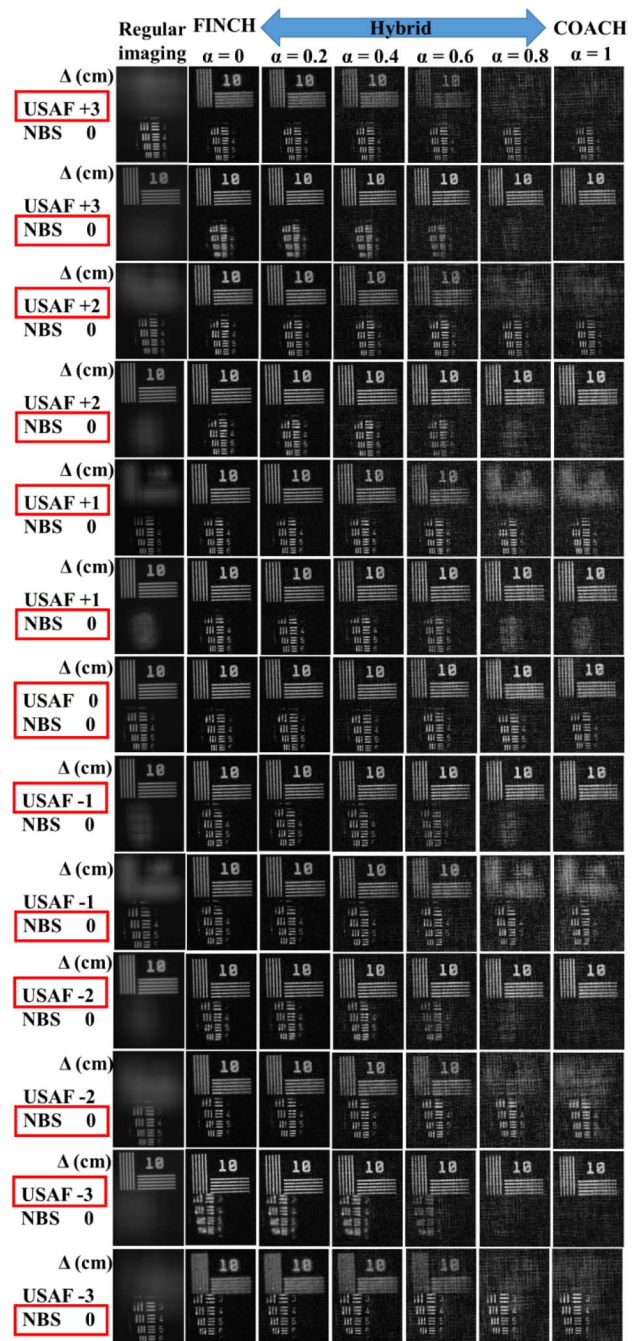


**Fig. 8.** Experimental comparison of results of regular imaging and reconstruction results of the hybrid system for  $\alpha = 0, 0.2, 0.4, 0.6, 0.8,$  and  $1$  for a two-plane object made up of the NBS resolution chart at plane 1 and the USAF resolution chart at plane 2 of channels 1 and 2, respectively, when the location of the USAF chart relative to the NBS chart was varied from  $\Delta = -3$  to  $3$  cm in steps of  $1$  cm. The red box represents the object and axial location that is in focus.

but with some background noise. The reconstruction by Fresnel backpropagation failed for higher values of  $\alpha$ . Because of power constraints, it is impossible in the present setup to work with a pinhole diameter below 25  $\mu\text{m}$ . Therefore, we conclude that with an ideal small pinhole it will

be possible to demonstrate the predicted higher lateral resolution of the hybrid system with  $\alpha < 1$ .

To analyze the behavior of the noise ratio with the change in  $\alpha$ , the ratio between the SNR for some  $\alpha$  and the SNR for  $\alpha = 1$  is defined as follows:

$$\frac{\text{SNR}_\alpha}{\text{SNR}_1} = \frac{\sigma_1}{\sigma_\alpha} = \frac{\sqrt{\frac{1}{MN} \sum_{m=1}^M \sum_{n=1}^N |P_1(m, n) - \bar{P}(m, n)|^2}}{\sqrt{\frac{1}{MN} \sum_{m=1}^M \sum_{n=1}^N |P_\alpha(m, n) - \bar{P}(m, n)|^2}},$$

$$\alpha = 0, 0.2, \dots, 1, \quad (13)$$

where  $\bar{P}(m, n)$ , in this case, is the average image chosen to be the reconstructed image from FINCH by Fresnel backpropagation. To analyze the change in the axial resolution versus  $\alpha$ , we define the ratio of the peak at  $z = 0$  to the average axial background as follows:

$$\text{PBR} = \frac{I(z = 0)}{\frac{1}{N} \sum_{z=-N/2}^{z=N/2} I(z)}. \quad (14)$$

The SNR and the peak-to-background ratio (PBR) of the axial curves (shown in Fig. 7) were calculated for different values of  $\alpha$  and plotted together in Fig. 9.

As expected, with the increase in the value of  $\alpha$ , the SNR decreases, while the PBR of the axial curve, which characterizes the axial resolution of the system, increases. This behavior of the SNR and PBR is obtained because a high value of  $\alpha$  means the system is more COACH-like with a lower SNR and a higher PBR, whereas a low value of  $\alpha$  means the system is more FINCH-like, with a higher SNR and a lower PBR. Figure 9 expresses the compromise of the hybrid system and can guide potential users to select the right  $\alpha$  value according to their choice of balance between noise and axial resolution. The demonstrated hybridization technique has indeed been proved useful for reduction of the background noise. However, the axial resolution of the system is decreased with the decrease in the background noise level. In some applications, a higher axial resolution is preferable, while in others, a lower axial resolution is necessary; therefore, by a correct choice of  $\alpha$ , the hybrid system can be tuned to different axial resolution values suitable for various applications.

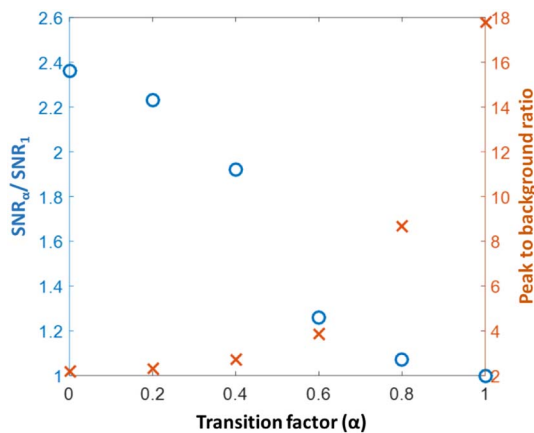


**Fig. 9.** Signal-to-noise ratio and peak-to-background ratio of the hybrid system for different values of the transition factor  $\alpha$ .

### C. Experimental Results of the Averaging Technique

Next the averaging method is used for reducing the background noise. The random-like CPM is the source for the higher axial resolution in COACH, while it is also the source for the background noise in the reconstruction plane. In the averaging approach, assuming that the background noise is a random signal with a zero mean, and assuming that the desired signal has a nonzero mean, one can improve the SNR by averaging over many independent COACH holograms, each of which is captured from different quasi-random CPMs. Even though each CPM is calculated by the GSA [20], the procedure starts with a different initial random phase mask, and therefore the final CPM is quasi-random, with relatively low cross correlation to any other CPM. Hence, in this approach, a library of CPMs was created and the COACH holograms for various objects ( $H_{\text{OBJ}}$ ) and for various pinholes ( $H_{\text{PSF}}$ ) were recorded using the different CPMs. In the end of the process, the multiple complex reconstructed images were averaged. Based on [37], it is expected that the SNR would be improved with an increase of the number of CPMs.

The experiment was repeated using two objects, USAF and NBS resolution charts located at different lateral planes. The axial location of the USAF resolution chart was varied from  $-3$  cm to  $+3$  cm with respect to the front focal plane of lens  $L_2$ , while the axial location of the NBS resolution chart was constant. This time, however, multiple holograms of the two objects were recorded corresponding to the different CPMs at every axial location of the USAF resolution chart. The experiment was repeated again using a pinhole with the same CPM library, such that the holograms  $H_{\text{PSF}}$  were recorded at the same axial locations as those of the USAF resolution chart. The regular imaging and reconstruction results for the object 10 lp/mm for FINCH, COACH, and COACH after averaging over the 20 reconstructions obtained with 20 different CPMs are shown in Fig. 10. The averaging technique is clearly effective in reducing the background noise of COACH.

A plot of the improvement in the SNR ratio ( $\text{SNR}_s / \text{SNR}_1$ ) when the number of CPMs was increased from  $s = 1$  to 20 and a theoretical  $\text{SNR}_s / \text{SNR}_1$  curve with a square-root dependence on  $s$  are shown in Fig. 11. The discrepancy between the theoretical and experimental curve in Fig. 11 is probably due to the increase in the coherence of the light during its propagation

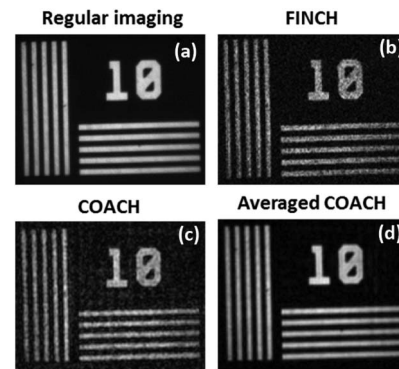


**Fig. 10.** Imaging results of (a) regular imaging, (b) FINCH, (c) COACH with a single CPM, and (d) averaged COACH with 20 different CPMs.

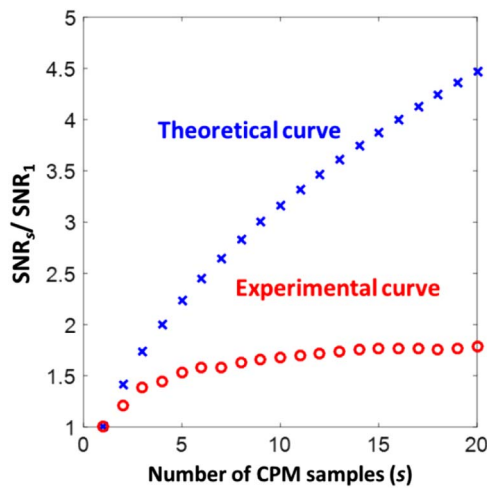


**Fig. 11.** Plot of the SNR for different numbers of CPM samples and the ideal SNR curve with square-root dependence on the number of samples.

from the SLM to the sensor plane. The square-root dependence on  $s$  is valid for random independent signals. However, it is well known that as the propagation distance becomes longer, the independence of the signals is reduced and hence the curve of the SNR improvement becomes different from the theoretical curve. Since the time resolution is inversely proportional to the number of exposures, Fig. 11 can also represent the dependence of the SNR versus the inverse of the time resolution. The reconstruction results after averaging over 5, 10, 15, and 20 samples are compared with those of COACH of a single CPM, FINCH, and regular imaging, as shown in Fig. 12. The results clearly demonstrate the decrease in the background noise, as well as the decrease in the out-of-focus noise, when the number of samples is increased from  $s = 1$  to 20. The demonstrated averaging technique reduces the background and the out-of-focus noise without affecting the axial resolution of the system. Hence, in a way, the averaging technique is better than the hybridization technique. The number of exposures required in the case of the averaging technique is quite high, which makes this technique time-consuming in some cases. However, it can be noted in Fig. 12 that as few as five samples are sufficient to obtain an SNR similar to FINCH. For any real application, the main parameter to consider is the SNR, from which the number of required samples can be deduced based on the curves in Fig. 11.

#### 4. SUMMARY AND CONCLUSIONS

In conclusion, we have presented a technique for reconstructing COACH holograms. The hologram of a point object is no longer used in its raw form as the reconstructing hologram. Instead, the reconstructing hologram, in this study, is computed as an inverse Fourier transform of the spectrum phase of the PSF hologram. Empirically, this modification improves the SNR of the reconstructed images. Further investigation is required in order to find the optimal filter of the reconstructing correlator, which might increase the SNR beyond the present results.

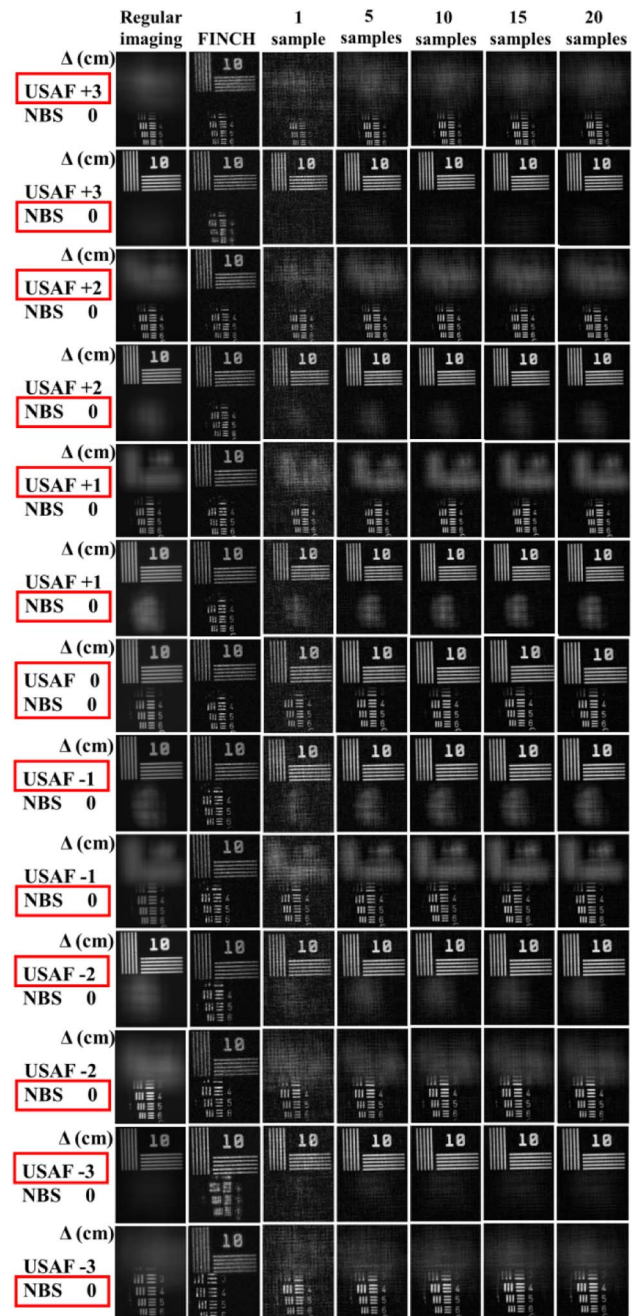


**Fig. 12.** Experimental results of COACH reconstruction with different numbers of CPMs ( $m = 1, 5, 10, 15, 20$ ), regular imaging, and FINCH reconstruction for a two-plane object made up of the NBS resolution chart at plane 1 and the USAF resolution chart at plane 2 of channels 1 and 2, respectively, when the location of the USAF chart relative to the NBS chart was varied from  $-3$  to  $3$  cm in steps of  $1$  cm. The red box represents the object and axial location that is in focus.

With this reconstructing hologram, we have proposed and demonstrated two methods of noise reduction in COACH. The hybrid method involves the integration of a quadratic phase mask, as used in FINCH, with a quasi-random CPM, as used in COACH. In this way, the hybrid system moves from FINCH to COACH through different levels of hybridization,

with associated hybrid properties of FINCH and COACH. Analysis of the hybrid system reveals the possibility of noise reduction by tuning the system from COACH toward FINCH. Even though the technique provides a solution to the background noise problem in COACH, the noise reduction occurs with the sacrifice of the axial resolution of the system. However, the hybrid system provides tunability to transfer the system in real time between different values of axial resolution and noise levels, which might be suitable for certain applications such as biological and industrial microscopy. The higher lateral resolution of FINCH, however, could not be realized in our experiments because such a high resolution demands a small pinhole size below the level that enables an acceptable SNR in the image sensor.

Another noise reduction technique has been proposed and demonstrated, where multiple holograms are recorded using independent quasi-random CPMs and their reconstructions are averaged. The background noise is decreased with an increase in the number of CPMs. This technique proved useful in noise reduction, while preserving the axial resolution of COACH. However, the process demands the recording of multiple independent holograms, and thus slows down the entire recording procedure.

**Funding.** Israel Science Foundation (ISF) (1669/16, 439/12); Ministry of Science and Technology, Israel.

## REFERENCES

- B. W. Schilling, T.-C. Poon, G. Indebetouw, B. Storrie, K. Shinoda, Y. Suzuki, and M. H. Wu, "Three-dimensional holographic fluorescence microscopy," *Opt. Lett.* **22**, 1506–1508 (1997).
- J. Rosen and G. Brooker, "Non-scanning motionless fluorescence three-dimensional holographic microscopy," *Nat. Photonics* **2**, 190–195 (2008).
- J. Rosen and G. Brooker, "Digital spatially incoherent Fresnel holography," *Opt. Lett.* **32**, 912–914 (2007).
- P. Bouchal, J. Kapitán, R. Chmelík, and Z. Bouchal, "Point spread function and two-point resolution in Fresnel incoherent correlation holography," *Opt. Express* **19**, 15603–15620 (2011).
- R. Kelner and J. Rosen, "Spatially incoherent single channel digital Fourier holography," *Opt. Lett.* **37**, 3723–3725 (2012).
- Y. Wan, T. Man, and D. Wang, "Incoherent off-axis Fourier triangular color holography," *Opt. Express* **22**, 8565–8573 (2014).
- M. K. Kim, "Adaptive optics by incoherent digital holography," *Opt. Lett.* **37**, 2694–2696 (2012).
- M. K. Kim, "Incoherent digital holographic adaptive optics," *Appl. Opt.* **52**, A117–A130 (2013).
- Y. Kashter and J. Rosen, "Enhanced-resolution using modified configuration of Fresnel incoherent holographic recorder with synthetic aperture," *Opt. Express* **22**, 20551–20565 (2014).
- Y. Kashter, Y. Rivenson, A. Stern, and J. Rosen, "Sparse synthetic aperture with Fresnel elements (S-SAFE) using digital incoherent holograms," *Opt. Express* **23**, 20941–20960 (2015).
- G. Brooker, N. Siegel, J. Rosen, N. Hashimoto, M. Kurihara, and A. Tanabe, "In-line FINCH super resolution digital holographic fluorescence microscopy using a high efficiency transmission liquid crystal GRIN lens," *Opt. Lett.* **38**, 5264–5267 (2013).
- D. Weigel, H. Babovsky, A. Kiessling, and R. Kowarschik, "Widefield microscopy with infinite depth of field and enhanced lateral resolution based on an image inverting interferometer," *Opt. Commun.* **342**, 102–108 (2015).
- J. Rosen and R. Kelner, "Modified Lagrange invariants and their role in determining transverse and axial imaging resolutions of self-interference incoherent holographic systems," *Opt. Express* **22**, 29048–29066 (2014).
- G. Indebetouw, "Scanning holographic microscopy with spatially incoherent sources: reconciling the holographic advantage with the sectioning advantage," *J. Opt. Soc. Am. A* **26**, 252–258 (2009).
- Y.-C. Lin, C.-J. Cheng, and T.-C. Poon, "Optical sectioning with a low-coherence phase-shifting digital holographic microscope," *Appl. Opt.* **50**, B25–B30 (2011).
- R. Kelner and J. Rosen, "Parallel-mode scanning optical sectioning using digital Fresnel holography with three wave interference phase-shifting," *Opt. Express* **24**, 2200–2214 (2016).
- R. Kelner, B. Katz, and J. Rosen, "Optical sectioning using a digital Fresnel incoherent-holography-based confocal imaging system," *Optica* **1**, 70–74 (2014).
- N. Siegel and G. Brooker, "Improved axial resolution of FINCH fluorescence microscopy when combined with spinning disk confocal microscopy," *Opt. Express* **22**, 22298–22307 (2014).
- A. Vijayakumar, Y. Kashter, R. Kelner, and J. Rosen, "Coded aperture correlation holography—a new type of incoherent digital holograms," *Opt. Express* **24**, 12430–12441 (2016).
- R. W. Gerchberg and W. O. Saxton, "A practical algorithm for the determination of phase from image and diffraction plane pictures," *Optik* **35**, 227–246 (1972).
- G. Z. Yang, B. Z. Dong, B. Y. Gu, J. Y. Zhuang, and O. K. Ersoy, "Gerchberg–Saxton and Yang–Gu algorithms for phase retrieval in a nonunitary transform system: a comparison," *Appl. Opt.* **33**, 209–218 (1994).
- R. H. Dicke, "Scatter-hole cameras for X-rays and Gamma rays," *Astrophys. J.* **153**, L101–L106 (1968).
- E. E. Fenimore and T. M. Cannon, "Coded aperture imaging with uniformly redundant array," *Appl. Opt.* **17**, 337–347 (1978).
- W. Chi and N. George, "Optical imaging with phase-coded aperture," *Opt. Express* **19**, 4294–4300 (2011).
- J. L. Horner and P. D. Gianino, "Phase-only matched filtering," *Appl. Opt.* **23**, 812–816 (1984).
- B. Javidi and T. Nomura, "Securing information by use of digital holography," *Opt. Lett.* **25**, 28–30 (2000).
- E. Tajahuerce and B. Javidi, "Encrypting three-dimensional information with digital holography," *Appl. Opt.* **39**, 6595–6601 (2000).
- G. Brooker, N. Siegel, V. Wang, and J. Rosen, "Optimal resolution in Fresnel incoherent correlation holographic fluorescence microscopy," *Opt. Express* **19**, 5047–5062 (2011).
- G. Indebetouw and W. Zhong, "Scanning holographic microscopy of three-dimensional fluorescent specimens," *J. Opt. Soc. Am. A* **23**, 1699–1707 (2006).
- C. Jang, D. C. Clark, J. Kim, B. Lee, and M. K. Kim, "Signal enhanced holographic fluorescence microscopy with guide-star reconstruction," *Biomed. Opt. Express* **7**, 1271–1283 (2016).
- J. Rosen, N. Siegel, and G. Brooker, "Theoretical and experimental demonstration of resolution beyond the Rayleigh limit by FINCH fluorescence microscopic imaging," *Opt. Express* **19**, 26249–26268 (2011).
- B. Katz, J. Rosen, R. Kelner, and G. Brooker, "Enhanced resolution and throughput of Fresnel incoherent correlation holography (FINCH) using dual diffractive lenses on a spatial light modulator (SLM)," *Opt. Express* **20**, 9109–9121 (2012).
- P. Bouchal and Z. Bouchal, "Wide-field common-path incoherent correlation microscopy with a perfect overlapping of interfering beams," *J. Eur. Opt. Soc.* **8**, 13011 (2013).
- J. B. Pawley, *Handbook of Biological and Confocal Microscopy* (Plenum, 1990).
- J. W. Goodman, *Statistical Optics* (Wiley, 1985).
- D. J. Goldstein, *Understanding the Light Microscope: a Computer Aided Introduction* (Academic, 1999).
- B. Katz, D. Wulich, and J. Rosen, "Optimal noise suppression in Fresnel incoherent correlation holography (FINCH) configured for maximum imaging resolution," *Appl. Opt.* **49**, 5757–5763 (2010).